Electrophoretic impregnation of porous anodic aluminum oxide film by silica nanoparticles

Benoit Fori[a,b], Pierre-Louis Taberna[a,*], Laurent Arurault[a], Jean-Pierre Bonino[a], Céline Gazeau[b], Pierre Bares[b]

[a] Université de Toulouse, CIRIMAT UPS-CNRS, 118 route de Narbonne, 31062 Toulouse Cedex 9, France
[b] Mecaprotec Industries, 34 Boulevard Joffrery, 31605 Muret Cedex, France

HIGHLIGHTS

- Pores of an anodic film were completely filled by electrophoretic impregnation.
- Electric field and dispersion conductivity control the impregnation depth.
- Progressive filling from the bottom of pores to the top.

GRAPHICAL ABSTRACT

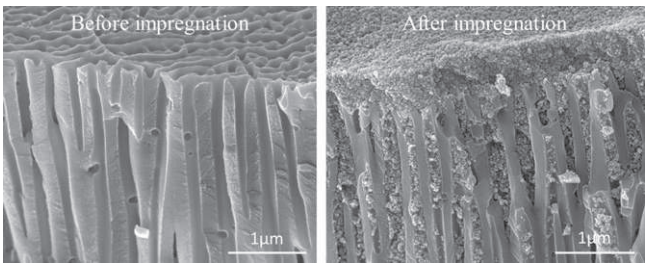

ABSTRACT

In this paper, it is proposed to study the deposition of nanoparticles by electrophoretic deposition (EPD) inside a porous anodic aluminum oxide film. Despite the presence of a highly resistive barrier layer at the metal-anodic film interface, porous anodic films on AA 1050A were successfully filled by 16-nm, surface modified silica particles. During this study it was shown that both the colloidal suspension conductivity and the applied electric field drive the penetration into the porous film. FEG-SEM observations showed that large (130-nm diameter), linear pores of 10 µm in length can be completely filled in 1 min. These results attest that porous anodic films can be efficiently filled with nanoparticles by EPD despite the presence of the barrier layer.

Keywords:
Electrophoretic deposition
Aluminum
Anodic film
Silica suspension

1. Introduction

Nanomaterials in the form of nanoparticles, nanowires and nanotubes are the main components in the burgeoning field of nanotechnology. Due to their physical and chemical properties, these nanoelements have the potential for use in applications such as memory devices [1], chemical sensors [2], medical science [3] and energy storage [4]. One promising technique to assemble these nanoelements over macroscopic length scales is the electrophoretic deposition (EPD) [5]. EPD is a well-established, versatile, low-cost method to deposit ceramic and metal films on a conducting substrate. This process deposits directly the end product avoiding chemical reactions at the surface of the substrate. However, the use of EPD in water is very restricted due to the electrolysis of water which occurs for low voltages and causes the evolution of hydrogen and oxygen gases at the electrodes which could affect the quality of the deposits formed [6].

Another advantage is that EPD can be used as well on flat surface as on complex surface. For example, Bazin et al. deposited silica nanoparticles by EPD on nanostructured copper electrodes to form

* Corresponding author. Tel.: +33 5 61 55 61 06; fax: +33 5 61 55 61 63.
E-mail address: taberna@chimie.ups-tlse.fr (P.-L. Taberna).

http://dx.doi.org/10.1016/j.colsurfa.2012.09.011

sensors [7]. Likewise numerous researchers [8–10] have studied the synthesis and the preparation of oxide nanorods and nanotubes by EPD using an anodic aluminum oxide membrane as template and fixed onto a metal foil. This technique consists to fill pores of the membrane by EPD and then to chemically remove the membrane. The resulting materials offer a significantly larger surface area than that of films or bulk material and thus find diverse application in nanotechnology (sensors, batteries, SOFC, etc.).

In contrast, very few studies have been devoted to the deposition of nanoparticles into unmodified porous anodic films i.e. including porous and compact layers still supported on aluminum substrate. Seo et al. [11] reported that pores can be partially filled by nanoparticles using the dip-coating process. But only a slight amount of nanoparticles were deposited at the bottom of pores with this method. As a result the quantity of nanoparticles into pores is too low to fill them completely. Because the migration of charged particles toward the pore bottom is promoted by applying an electric field, the EPD technique should increase the density of particles in comparison with the dip-coating process.

To demonstrate the feasibility of such process, silica nanoparticles were chosen as model charged particles. EPD of silica is an easy process because silica suspensions are characterized by spherical particles and a high negative zeta potential, providing good stability of the suspension and efficient migration [7,12]. Another advantage is that silica surface can be functionalized with various organic molecules, providing new properties to particles [13].

To our knowledge, Kamada et al. [14] studied for the first time the insertion of SiO_2 nanoparticles into pores of anodized aluminum by electrophoretic deposition. However, they used an aqueous silica solution and their characterizations (e.g. EPMA profiles) showed an uncompleted filling in the pores.

In this paper we proposed to deeply study the electrophoretic deposition of silica nanoparticles into pores of an unmodified anodic film of 10 μm of thickness. It is generally assumed that the presence of a conducting surface increases the efficiency of the EPD. Completely filling porous anodic film appears therefore as a challenge because of the resistive barrier layer below the pores. Furthermore one of our wills in this work is the elucidation of the mechanism of particle migration and deposition into the pores which is very few discussed into the literature. Thus in a first step, an aluminum porous anodic film suitable to the electrophoretic impregnation will be prepared. In a second step the influence of the applied voltage and the suspension conductivity on the pores filling by grafted SiO_2 particles using EPD will be studied.

2. Material and methods

2.1. Preparation of the anodic film

To facilitate the insertion of particles inside pores, the porosity of the anodic films has to exhibit low tortuosity and pore diameter larger than the silica particle one (15 nm). 1050A aluminum alloy (chemical composition in weight percent: 99.5% Al, <0.40% Fe, <0.25% Si, <0.05% Cu) was used as a substrate to get linear pores perpendicular to the initial metal surface [15]. Since large pores (average pore diameter >100 nm) are required, a phosphoric acid based electrolyte was chosen as anodizing bath [16].

First the alloy sheet (20 mm × 20 mm × 1 mm) was degreased with ethanol. Secondly the sample was etched in NaOH (0.5 g L^{-1}) aqueous solution at 40 °C for 5 min and then neutralized in HNO_3 (25 vol%) at room temperature for 2 min; water used to make these solutions exhibit a resistivity of 10 Ω cm^{-1}. Thirdly the aluminum sheet was used as anode and a lead plate (3 mm × 40 mm × 40 mm) as counter-electrode in the electrochemical cell. The anodizing was run in the galvanostatic mode (TDK-Lambda GEN 300-5) using a temperature controlled phosphoric acid solution (0.4 mol L^{-1}). The samples were rinsed in deionized water (10 kΩ cm^{-1}) immediately at the end of each step.

2.2. Electrophoretic impregnation

A commercial colloidal suspension of silica nanoparticles (15 nm) in isopropyl alcohol (ABCR, Germany) was used. This suspension was diluted with isopropyl alcohol (Carlo Erba, Italy) to obtain a concentration of about 15 g L^{-1} and vigorously stirred. Functionalization of silica was achieved following Cousinié et al. [17]. 3 ml of aminopropyltrimethoxysilane (APTMS) was added dropwise in 100 mL of the diluted suspension. The mixture was then vigorously stirred for three days and then diluted 100 times with isopropyl alcohol leading to a concentration of about 0.15 g L^{-1}. 1–15 mL of an I_2–acetone mixture (6 g L^{-1}) was added to the as-prepared suspension [18]. In order to carry out the electrophoretic deposition the anodized aluminum was set as the cathode; the lead foil, as the anode. The substrate was dried at ambient temperature after experiment.

2.3. Characterizations

A field emission gun scanning electron microscope (FEG-SEM, JEOL JSM 6700F) was used to observe the microstructure of the coatings. The average impregnation depth was measured on the FEG-SEM views using the free software ImageJ.

MALVERN NANOSIZER ZS90 was used for zeta potential measurements and Stokes particle diameter measurements using dynamic light scattering (DLS).

3. Results and discussion

3.1. Tuning of the film porosity

The diameter of the commercial silica nanoparticles used for EPD is announced to be equal to 15 nm. It seems obvious that the pore has to exhibit a larger diameter than particles to allow their insertion. Therefore an anodic film with pore larger than 100 nm should be suitable for the electrophoretic impregnation. So operating parameters (temperature, current density, duration) of the anodizing are studied in order to adequately tune the characteristics of the anodic film on the aluminium substrate.

3.1.1. Influence of the temperature

To study the influence of the electrolyte temperature, the current density was fixed at 1.5 A dm^{-2} and the anodization time at 2400 s. The samples were anodized at 5 °C, 15 °C, 25 °C and 35 °C.

Fig. 1a shows the influence of the electrolyte temperature on the pore diameter and the pore density. Between 5 °C and 35 °C, the pore diameter and the pore density increase with electrolyte temperature. At 5 °C the pores have an average diameter of 110 ± 10 nm and the pore density is equal to $(8.9 \pm 5.0) \times 10^{12}$ pores m^{-2} whereas the pore diameter is 205 ± 10 nm and the pore density is $(1.7 \pm 0.5) \times 10^{13}$ pores m^{-2} at 35 °C.

The increase of the electrolyte temperature typically increases reaction kinetics. The anodic film growth occurs through two main opposite processes: an aluminum electro-oxidation according to reaction (1); a chemical dissolution (reaction (2)) of the anodic film by the acidic electrolyte.

$$2Al + 3H_2O \rightarrow Al_2O_3{\cdot}xH_2O + 6H^+ + 6e^- \quad (1)$$

$$Al_2O_3{\cdot}xH_2O + 6H^+ \rightarrow 2Al^{3+} + (3+x)H_2O \quad (2)$$

So, the increase of the electrolyte temperature increases the dissolution rate and leads to the formation of wider pores [19]. Also,

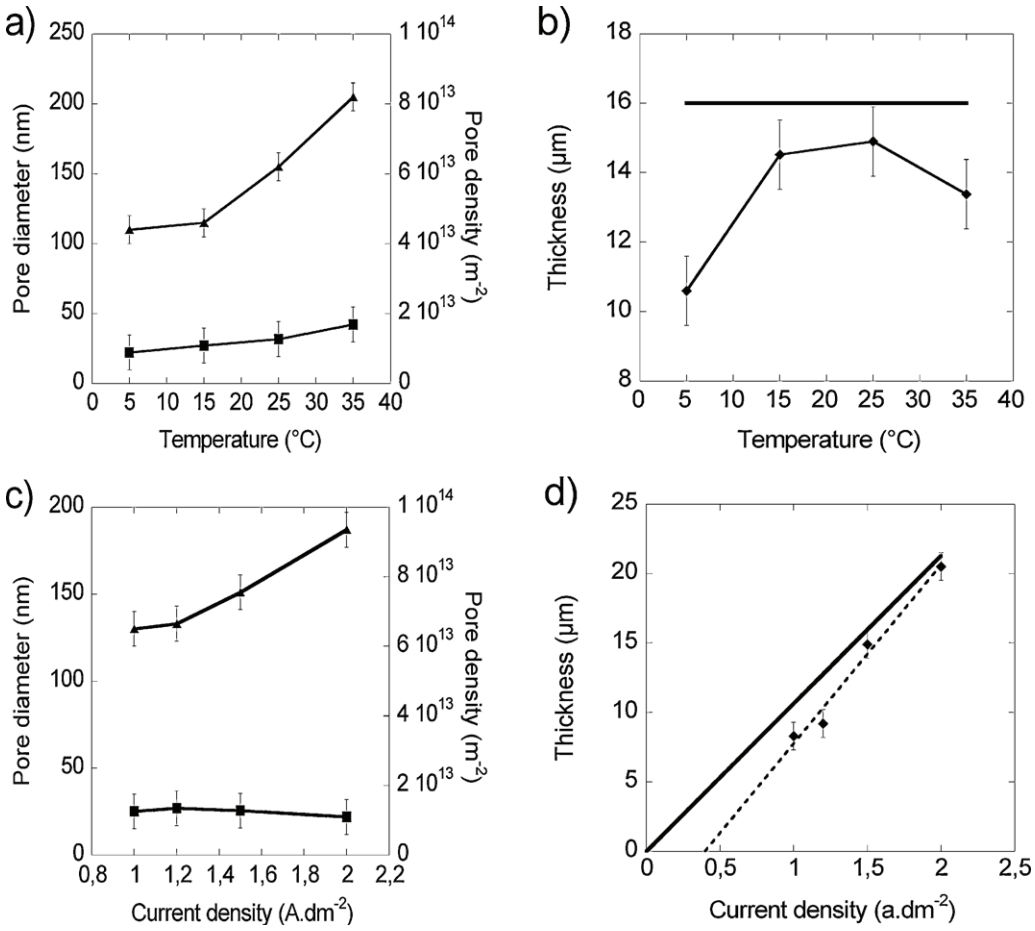

Fig. 1. Pore diameter (▲), pore density (■), experimental thickness (♦) and theoretical thickness (—) versus the temperature (a, b) and the current density (c, d) (duration: 2400 s).

the pore densities of this study are close to the values obtained under similar operating conditions and presented in other works [20,21].

Usually the film thickness is predicted through Eq. (3), based on the Faraday's law:

$$h = \frac{Mjt}{nF\rho} \tag{3}$$

where h is the height of the anodic film, M the molar weight of the anodic film ($M = 102\,\mathrm{g\,mol^{-1}}$ for Al_2O_3), j the current density ($j = 1.5\,\mathrm{A\,dm^{-2}}$ in our conditions), t the anodizing duration ($t = 2400\,\mathrm{s}$ in our conditions), n the number of electron exchanged during the reaction ($n = 6$), F the Faraday constant ($F = 96485\,\mathrm{C\,mol^{-1}}$) and ρ the specific density of the anodic film ($\rho = 3.97\,\mathrm{g\,cm^{-3}}$). According to this relation, the predicted thickness should be constant (here about 16 μm) whatever the electrolyte temperature. However, Fig. 1b reveals that the thickness of the anodic film, measured by SEM, increases from 10.6 ± 0.1 μm to 14.9 ± 0.1 μm between 5 °C and 25 °C and then decreases. Similar behavior was obtained by Goueffon et al. [21] and Shih and Tzou [22].

During anodizing a competition between the electrochemical growth of the film (reaction (1)) and its chemical dissolution by the acidic electrolyte occurs (reaction (2)). The temperature influences a chemical reaction more than an electrochemical one. So the change of the thickness versus the electrolyte temperature is mainly due to the dissolution reaction, which is not considered in Faraday's law. When the temperature is too high the pore diameter is so large that the pore walls disappear leading to pore interconnection, mechanical fragility and finally to collapse of the film thickness.

In order to prepare a suitable anodic film for electrophoretic impregnation, an electrolyte temperature of 25 °C was used. This temperature gives large pores (about 150 nm) and simultaneously avoids collapse of the film.

3.1.2. Influence of the current density

This study was performed at 25 °C and an anodizing time of 2400 s. The samples were anodized at $1.0\,\mathrm{A\,dm^{-2}}$, $1.2\,\mathrm{A\,dm^{-2}}$, $1.5\,\mathrm{A\,dm^{-2}}$ and $2.0\,\mathrm{A\,dm^{-2}}$. The voltage measured in steady-state conditions of the anodization was respectively of 121 V, 127 V, 132 V and 141 V.

Fig. 1c shows the evolution of the pore diameter and the pore density in the 1.0–2.0 $\mathrm{A\,dm^{-2}}$ range. The pore diameter increases with the current density, whereas the pore density remains constant. Similar behaviors were obtained by O'Sullivan and Wood [23] and Ono and Masuko [16]. The increase of the pore diameter can be explained by field-assisted dissolution of the anodic film. At the base of the pore, the density of the current lines increases leading to a local temperature increase which promotes the dissolution of the anodic film and thus the increase of the pore diameter [23].

Fig. 1d highlights a linear correlation between the thickness and the current density. The straight line does not pass by the origin in disagreement with Faraday's law. Indeed at low current density ($<0.3\,\mathrm{A\,dm^{-2}}$) the dissolution reaction dominates electrochemical film growth.

A current density of $2.0\,\mathrm{A\,dm^{-2}}$ gives larger pores at the risk of local over heating (also called "burning phenomenon") leading

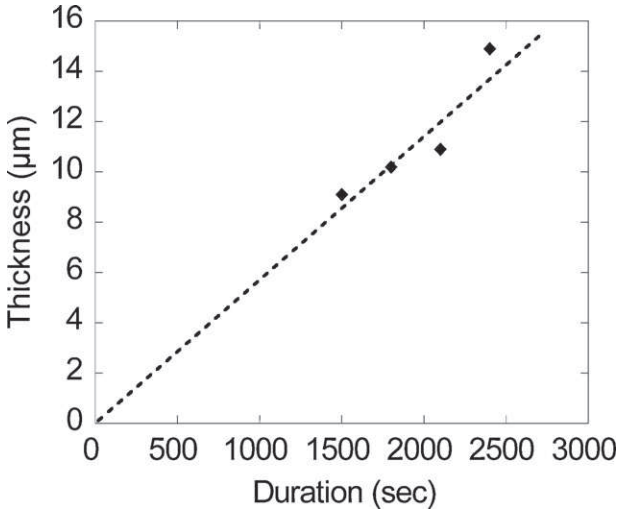

Fig. 2. Thickness of the anodic film versus duration ($T = 25\,^{\circ}C$, $j = 1.5\,A\,dm^{-2}$).

to non-homogenous porous oxide layer increases. So in order to achieve a porous anodic film suitable to the electrophoretic impregnation, a current density of $1.5\,A\,dm^{-2}$ was used.

3.1.3. Characteristics of the standard anodic film

The thickness of the anodic film was measured versus anodization duration. It appears that it is proportional to duration as expected with the Faraday's law. In order to study the migration of the particles into the pores, it has been decided to prepare a thick anodic film of 10 μm. According to Fig. 2, duration of 29 min is required to obtain this thickness and consequently to form the standard anodic film. To sum up, anodizing is performed on AA 1050 in the following operational conditions: galvanostatic mode ($1.5\,A\,dm^{-2}$) in $0.4\,mol\,L^{-1}$ phosphoric acid electrolyte at 25 °C for 29 min.

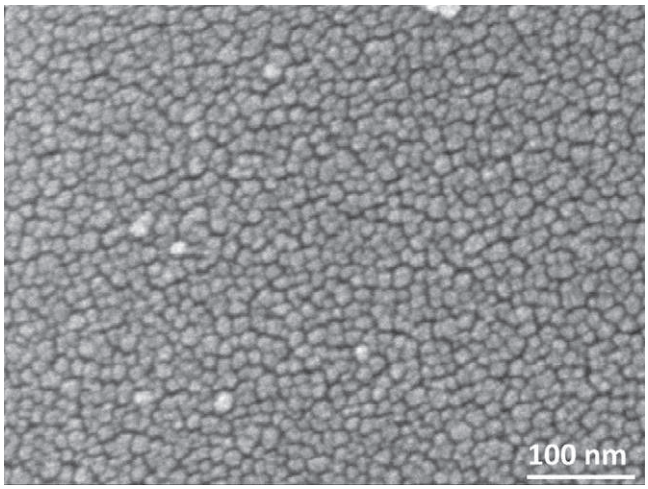

Fig. 4. FEG-SEM view of the silica nanoparticles.

The standard films have large linear pores making them suitable for electrophoretic impregnation. FEG-SEM plan view of the as-prepared anodic film shows that the porosity is well formed, the pore diameter being 130 ± 10 nm (Fig. 3a). Le Coz et al. prepared anodic film with pore diameter of the same order of magnitude [24]. The cross sectional view (Fig. 3b) confirms that the pores are orthogonal to the AA substrate and that the film has a thickness of 10 ± 1 μm. The barrier layer thickness is 130 ± 5 nm (Fig. 3c) which is consistent with Vrublevsky et al. [25].

3.2. Preparation of the silica colloidal suspension

Electrophoresis can be performed in aqueous or organic solvent. Since higher electric fields are reachable in organic solvents, isopropyl alcohol was chosen. Silica suspensions were used because they have high stability and can be functionalized easily due to their high surface reactivity. Indeed Si–OH groups at the particles

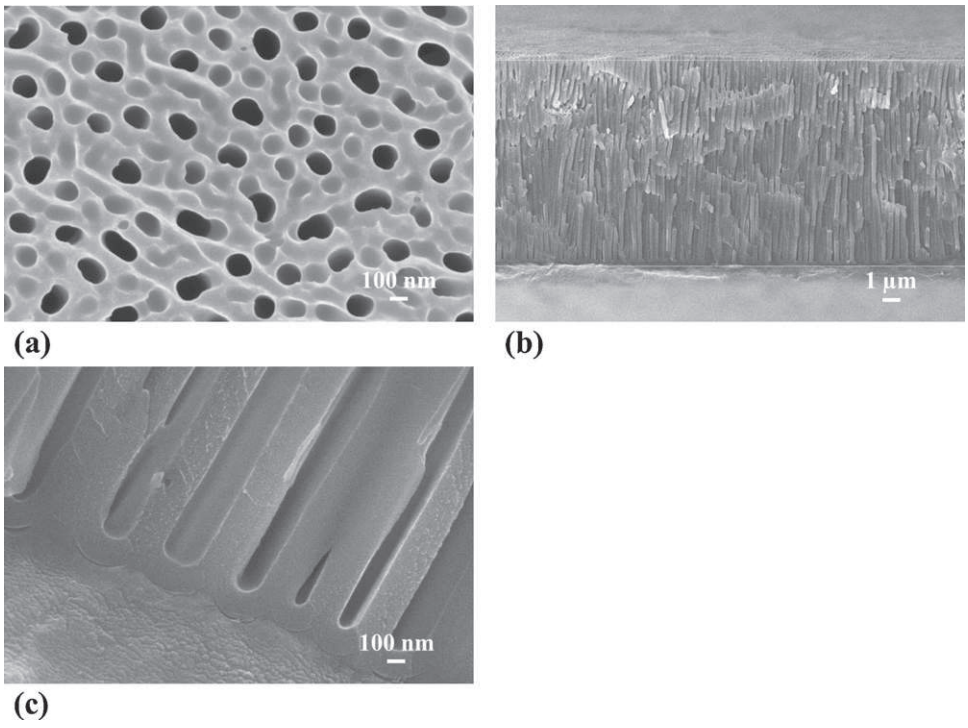

Fig. 3. FEG-SEM plan (a) and cross sectional (b, c) views of the standard porous anodic film ($T = 25\,^{\circ}C$, $j = 1.5\,A\,dm^{-2}$, duration: 29 min).

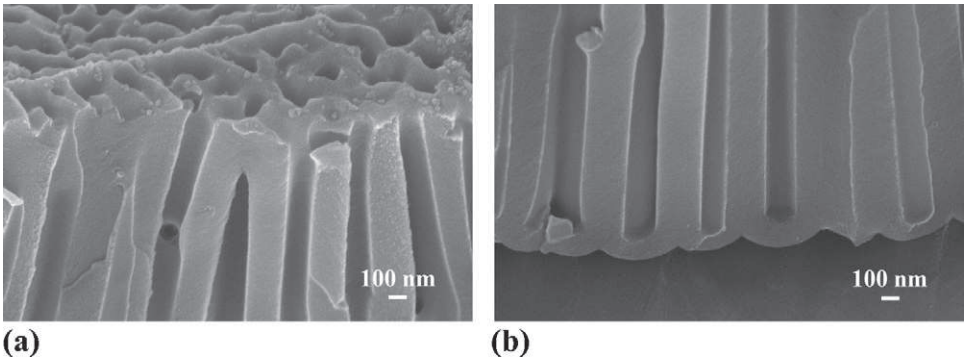

Fig. 5. FEG-SEM cross sectional view of the top (a) and the bottom (b) of the porous anodic film after the immersion into the suspension.

surface can form covalent bonds with organic molecules having alkoxysilane or chlorosilane groups. The organic molecules have other organic functions whose physical or/and chemical properties can be transmitted to the silica particle. During electrophoresis, the anodized aluminum was the cathode for two reasons. Firstly the aluminum foil can be over-oxidized if used as an anode thus it can modify its morphology [26]. Secondly, by applying a cathodic polarization, the barrier layer of the anodic film acts as an n-type semi-conductor, so current can pass through [27]. Electing the cathodic mode for the electrophoretic deposition, the silica particles must have positive surface charge in order to migrate toward the cathode.

A commercial colloidal suspension of silica nanoparticles in isopropanol (SiO_2-COM) was used. The nanoparticles exhibit an average diameter of 13 nm (Fig. 4). The initial zeta potential was measured at -40 ± 10 mV. To get a positive potential we used a two-step functionalization. Firstly aminopropyltrimethoxysilane (APTMS) was grafted onto silica surface. This organic species has a positively charged amine group [13,17]. Secondly an I_2–acetone mixture was added to the suspension. One of the advantages of this method is to create some positives charges in organic media without adding water [18]. Acetone generates H^+ ions by a keto-enol reaction catalyzed by the oxide surface (Eqs. (4) and (5)).

$$CH_3COCH_3 \leftrightarrow CH_3C(OH)CH_2 \quad (4)$$

$$CH_3C(OH)CH_2 + I_2 \rightarrow CH_3COCH_2I + H^+ + I^- \quad (5)$$

The H^+ so formed are adsorbed on the silica particles and/or reacts with the amino group of the ligands; both of these phenomena make the particles positively charged. Then the functionalized silica suspension (SiO_2-FUNC) shows a zeta potential of $+30 \pm 10$ mV. The measured average diameter was 16 ± 1 nm. This diameter is close to the diameter of the commercial suspension confirming that no further aggregation was noticed. Moreover

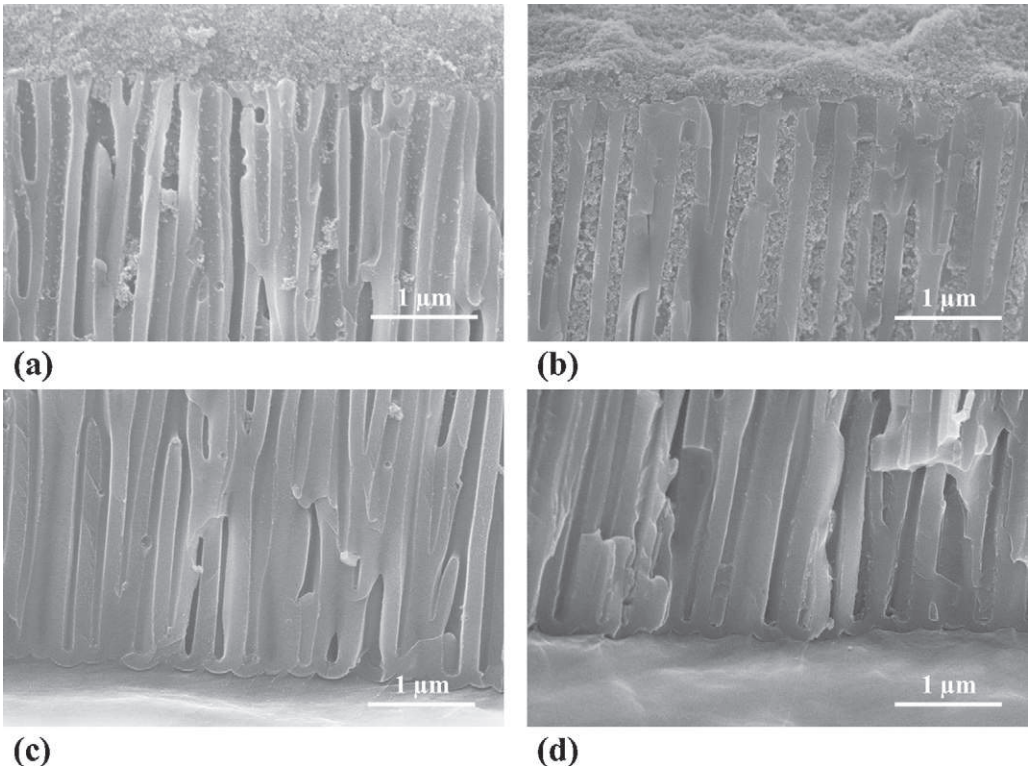

Fig. 6. FEG-SEM cross sectional views of the porous anodic film after the electrophoresis process using 33 V cm^{-1} (top (a) and bottom (c) of the pores) and 200 V cm^{-1} (top (b) and bottom (d) of the pores) for 5 min (suspension conductivity: 74 µS cm^{-1}).

the diameter is well below the aluminum oxide pore diameter (130 ± 10 nm).

3.3. Electrophoretic impregnation

3.3.1. Impregnation without polarization

For comparison an impregnation was realized by dip-coating, it is to say without any electric field. The substrate was soaked into the colloidal suspension for 5 min and then withdrawn from the silica suspension. Fig. 5 shows FEG-SEM cross sectional view of the top and the bottom of the anodic film after the dipping. These micrographs show that just a few particles are present on the top of the film but no particles are inside the pores.

During drying, solvent evaporation induces a convective motion of the particles toward the surface of the anodic film where adsorption occurs. Simultaneously an increase of the particle concentration occurs at the solvent–film interface. Above a critical concentration, aggregation occurs and the particles deposit onto the film explaining the presence of particles at the top of the pores. This experiment reveals that simple immersion does not permit filling the pores.

3.3.2. Influence of the electric field

Several electric fields ($33\,V\,cm^{-1}$, $66\,V\,cm^{-1}$, $133\,V\,cm^{-1}$, $200\,V\,cm^{-1}$) were applied for 5 min in order to study its influence on the electrophoretic impregnation (suspension conductivity: $74\,\mu S\,cm^{-1}$). FEG-SEM cross sectional views reveals that electric field improves insertion of particles inside pores (Fig. 6). When an electric field of $33\,V\,cm^{-1}$ is applied, particles deposit only at the top of the pores, whereas particles are present inside pores with an electric field of $200\,V\,cm^{-1}$. The changes of the average impregnation depth versus the applied voltage are summarized in Fig. 7. No particles are deposited at the bottom of pores however.

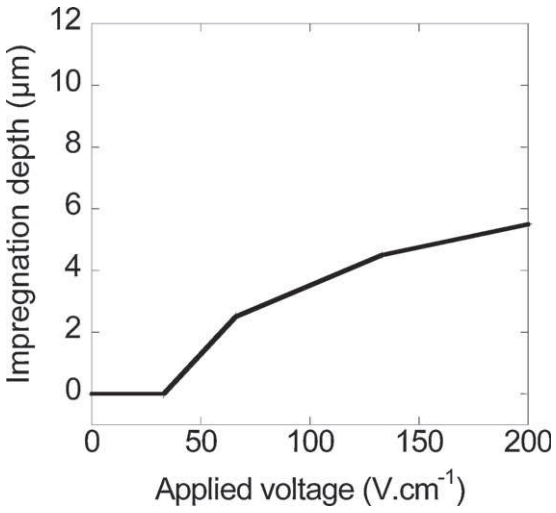

Fig. 7. Impregnation depth versus the applied voltage (suspension conductivity: $75\,\mu S\,cm^{-1}$, duration: 5 min).

3.3.3. Influence of the suspension conductivity

The influence of the suspension conductivity was also studied using an electric field of $200\,V\,cm^{-1}$ for 5 min. To change the conductivity different volumes of an I_2–acetone mixture ($6\,g\,L^{-1}$) were added to the suspension. FEG-SEM cross sectional views show that low suspension conductivity ($40\,\mu S\,cm^{-1}$) leads to the formation of a deposit at the surface of the pores (Fig. 8a and c) whereas an increase of the suspension conductivity allows complete filling of the pores (Fig. 11b and d). The changes of the penetration depth versus the suspension conductivity are summarized in Fig. 9. The saturation of the impregnation depth for conductivities higher than $120\,\mu S\,cm^{-1}$ corresponds to the complete filling of the anodic film.

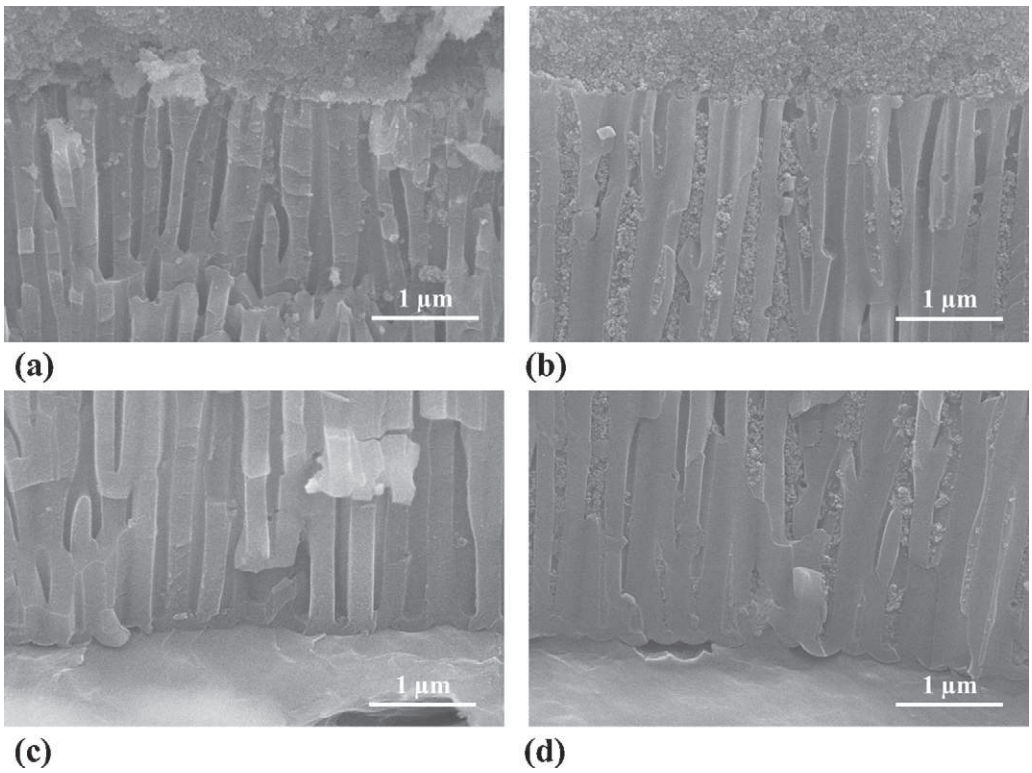

Fig. 8. FEG-SEM cross sectional views of the porous anodic film after the electrophoresis process using $200\,V\,cm^{-1}$ during 5 min with two different suspension conductivity: $40\,\mu S\,cm^{-1}$ (top (a) and bottom (c) of the pores) and $120\,\mu S\,cm^{-1}$ (top (b) and bottom (d) of the pores).

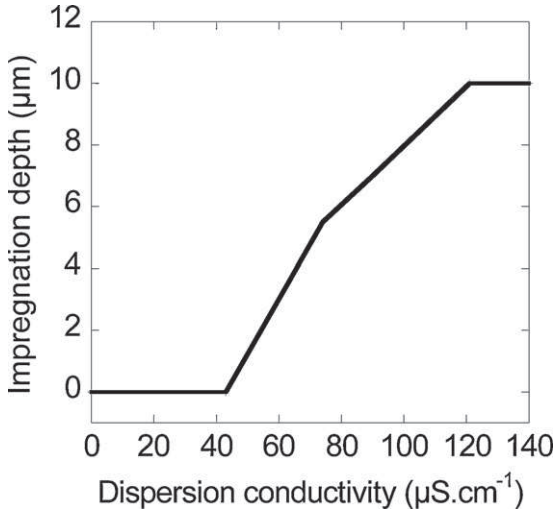

Fig. 9. Impregnation depth versus the suspension conductivity (200 V cm^{-1}, duration: 5 min).

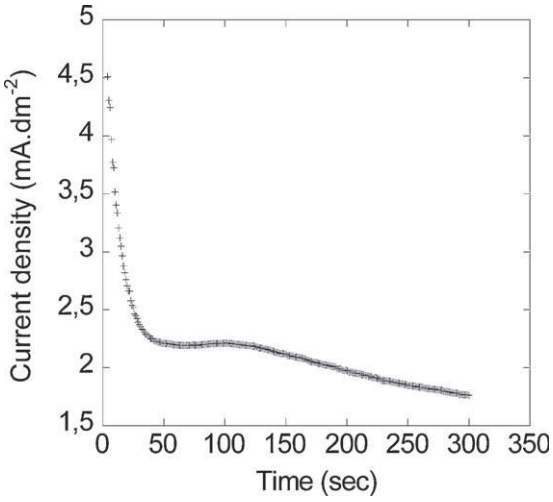

Fig. 10. Current density versus deposition time for deposition of silica particles at 200 V cm^{-1} during 5 min (suspension conductivity: 120 µS cm^{-1}).

3.3.4. Study of the electrophoretic pore filling

To fill entirely the pores, an electric field of 200 V cm^{-1} was applied for 5 min with a suspension conductivity of 120 µS cm^{-1}. The conductivity was measured before and after electrophoresis. Initially it was equal to 120 µS cm^{-1} and decreases to 95 µS cm^{-1} after the impregnation. The current was also measured during electrophoresis (Fig. 10). At the beginning of the experiment the current density decreases then increases a little bit (or stabilizes) before ending up decreasing again. Since the conductivity of the suspension does not change more than 20%, the first decrease of the current (between 0 s and 50 s) probably corresponds to an increase of the resistivity of the film due to the aggregation of particles at the surface and inside the pores. It is reported in the literature that this resistance deposit is caused by the formation of an ion depletion layer in the deposit [28] and mass transport limitations through the growing deposit layer [29]. The small increase (or stabilization) between 50 s and 100 s can be due to the dielectric breakdown of the initial insulating anodic film.

In order to know the chronology of the deposit, FEG-SEM micrographies were made at different electrophoresis times. Fig. 11 reveals that particles are present only at the bottom of the pores after 15 s whereas pores are completely filled by particles after 1 min. At the beginning of the electrophoresis, particles go to the bottom of the pores and then progressively fill the pores entirely.

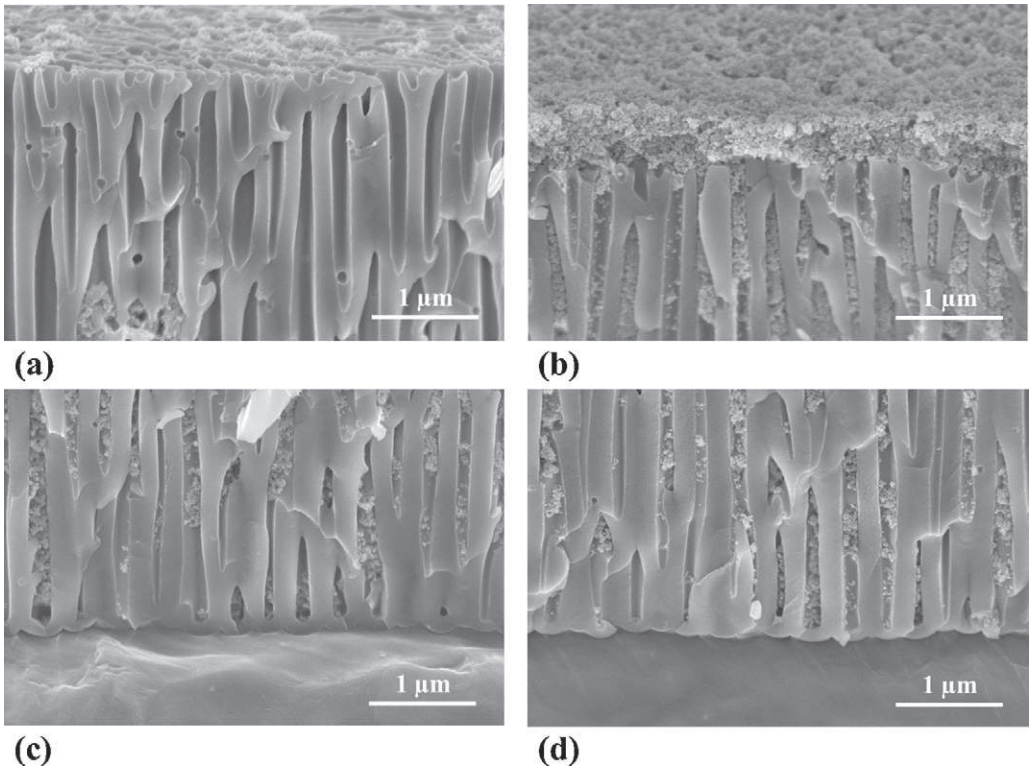

Fig. 11. FEG-SEM cross sectional views of the porous anodic film after the electrophoresis process using 200 V cm^{-1} during 15 s (top (a) and bottom (c) of the pores) and 60 s (top (b) and bottom (d) of the pores).

During electrophoresis the current lines pass through the barrier layer and not through the too resistive pore walls. Therefore the particles go to the bottom of the pores and fill the pores as the electrophoresis process continues. Once the pores are filled, particles deposit on the surface.

As shown in Figs. 6 and 7 an increase of the electric field improves the impregnation depth of particles. These observations reveal that a high electric field is likely needed during electrophoresis to avoid aggregation of particles at the top of pores. An important electric field is required here because of the presence of the resistive barrier layer at the metal-porous anodic film interface. The migration speed of the particles is described by the following equation:

$$v = \mu E \tag{6}$$

with v the speed of the particles ($m\,s^{-1}$), μ the electrophoretic mobility of the particles ($m^2\,s^{-1}\,V^{-1}$) and E the electric field ($V\,m^{-1}$). According to Eq. (6) an increase of the electric field enhances the driving forces of particles and so facilitates their insertion inside pores.

An increase of the conductivity improves the electrophoretic impregnation too (Figs. 8 and 9). These results can be explained by the establishment of a higher potential gradient through the anodic film [30]. The principal driving force of particles for EPD is the applied electric field. So high potential gradient across the anodic film is required to allow the insertion of particles inside pores. If the suspension has a low conductivity, the potential gradient is mainly located into the resistive suspension and particles cannot enter inside pores due to the weak potential gradient in the anodic film region. So an increase of the suspension conductivity transfers the potential gradient from the bulk suspension to the barrier layer region by reducing the potential drop in the suspension. Therefore an increase of the conductivity concentrates the electric field in the anodic film making insertion of the particle inside pores easier. Moreover an increase of the suspension conductivity promotes the thinning of the electrical double layer at pore walls enhancing mass transport through the pore [31]. Therefore it appears through these results that the conductivity is likely to be one of the most important parameter to fill porous anodic film by EPD.

4. Conclusion

Electrophoretic impregnation of porous anodic film formed in phosphoric acid based electrolyte was performed in an organic SiO_2 colloidal suspension. Indeed almost all pores have been completely filled by grafted APTMS-SiO_2. The electric field and the suspension conductivity are two key factors that control the impregnation. At the beginning of EPD, particles go to the bottom of pores which continue to fill progressively. These results attest that EPD can be used to fill successfully porous anodic film despite the presence of the resistive barrier layer at the metal–oxide interface.

Acknowledgements

This work was financially supported by MECAPROTEC Industries. We thank B. Daffos and P. Lenormand for the FEG-SEM pictures.

References

[1] T. Rueckes, K. Kim, E. Joselevich, G.Y. Tseng, C.L. Cheung, C.M. Liebe, Carbon nanotube-based nonvolatile random access memory for molecular computing, Science 289 (2000) 94–97.
[2] C. Li, D. Zhang, X. Liu, S. Han, T. Tang, J. Han, C. Zhoub, In_2O_3 nanowires as chemical sensors, Appl. Phys. Lett. 82 (2003) 1613–1615.
[3] L.R. Hirsch, R.J. Stafford, J.A. Bankson, S.R. Sershen, B. Rivera, R.E. Price, J.D. Hazle, N.J. Halas, J.L. West, Nanoshell-mediated near-infrared thermal therapy of tumors under magnetic resonance guidance, Proc. Natl. Acad. Sci. U.S.A. 100 (2003) 13549–13554.
[4] P.L. Taberna, S. Mitra, P. Poizot, P. Simon, J.M. Tarascon, High rate capabilities Fe_3O_4-based Cu nano-architectured electrodes for lithium-ion battery applications, Nat. Mater. 5 (2006) 567–573.
[5] L. Besra, M. Liu, A review on fundamentals and applications of electrophoretic deposition (EPD), Prog. Mater. Sci. 52 (2006) 1–61.
[6] L. Besra, T. Uchikoshi, T.S. Suzuki, Y. Sakka, Application of constant current pulse to suppress bubble incorporation and control deposit morphology during aqueous electrophoretic deposition (EPD), J. Eur. Ceram. Soc. 29 (2009) 1837–1845.
[7] L. Bazin, M. Gressier, P.L. Taberna, M.J. Menu, P. Simon, Electrophoretic silica-coating process on a nano-structured copper electrode, Chem. Commun. (2008) 5004–5006.
[8] G. Cao, D. Liu, Template-based synthesis of nanorod, nanowire, and nanotube arrays, Adv. Colloid Interface Sci. 136 (2008) 45–64.
[9] A. Nourmohammadi, M. Bahrevar, M. Hietschold, Template-based electrophoretic deposition of perovskite PZT nanotubes, J. Alloys Compd. 473 (2009) 467–472.
[10] E. Gultepe, D. Nagesha, L. Menon, High-throughput assembly of nanoelements in nanoporous alumina templates, Appl. Phys. Lett. 90 (2007) 163119.
[11] I. Seo, C.W. Kwon, H.H. Lee, Y.S. Kim, K.B. Kim, T.S. Yoon, Completely filling anodic aluminum oxide with maghemite nanoparticles by dip-coating and their magnetic properties, Electrochem. Solid-State Lett. 12 (2009) K59–K62.
[12] K. Grandfield, I. Zhitomirsky, Electrophoretic deposition of composite hydroxyapatite–silica–chitosan coatings, Mater. Charact. 59 (2008) 61–67.
[13] Z. Csogör, M. Nacken, M. Sameti, C.M. Lehr, H. Schmidt, Modified silica particles for gene delivery, Mater. Sci. Eng. C 23 (2003) 93–97.
[14] K. Kamada, H. Fukuda, K. Maehara, Y. Yoshida, M. Nakai, S. Hasuo, Y. Matsumoto, Insertions of SiO_2 nanoparticles into pores of anodized aluminum by electrophoretic deposition in aqueous system, Electrochem. Solid-State Lett. 7 (2004) B25–B28.
[15] S. Garcia-Vergara, K. El Khazmi, P. Skeldon, G.E. Thompson, Influence of copper on the morphology of porous anodic alumina, Corros. Sci. 48 (2006) 2937–2946.
[16] S. Ono, N. Masuko, Evaluation of pore diameter of anodic porous films formed on aluminum, Surf. Coat. Technol. 169–170 (2003) 139–142.
[17] S. Cousinié, M. Gressier, P. Alphonse, M.J. Menu, Silica-based nanohybrids containing dipyridine, urethan or urea derivatives, Chem. Mater. 19 (2007) 6492–6503.
[18] I. Zhitomirsky, Cathodic electrophoretic deposition of diamond particles, Mater. Lett. 37 (1998) 72–78.
[19] T. Aerts, T. Dimogerontakis, I. De Graeve, J. Fransaer, H. Terryn, Influence of the anodizing temperature on the porosity and the mechanical properties of the porous anodic oxide film, Surf. Coat. Technol. 201 (2007) 7310–7317.
[20] A. Tamburrano, B. De Vivo, M. Höijer, L. Arurault, V. Tucci, S. Fontorbes, P. Lamberti, V. Vilar, B. Daffos, M.S. Sarto, Effect of electric field polarization and temperature on the effective permittivity and conductivity of porous anodic aluminium oxide membranes, Microelectron. Eng. 88 (2011) 3338–3346.
[21] Y. Goueffon, L. Arurault, S. Fontorbes, C. Mabru, C. Tonon, P. Guigue, Chemical characteristics, mechanical and thermo-optical properties of black anodic films prepared on 7175 aluminium alloy for space applications, Mater. Chem. Phys. 120 (2010) 636–642.
[22] H. Shih, S. Tzou, Study of anodic oxidation of aluminum in mixed acid using a pulsed current, Surf. Coat. Technol. 124 (2000) 278–285.
[23] J. O'Sullivan, G. Wood, The morphology and mechanism of formation of porous anodic films on aluminium, Proc. Roy. Soc. Lond. A 317 (1970) 511–543.
[24] F. Le Coz, L. Arurault, L. Datas, Chemical analysis of a single basic cell of porous anodic aluminium oxide template, Mater. Charact. 61 (2010) 283–288.
[25] I. Vrublevsky, V. Parkoun, J. Schreckenbach, Analysis of porous oxide film growth on aluminum in phosphoric acid using re-anodizing technique, Appl. Surf. Sci. 242 (2005) 333–338.
[26] K. Kamada, M. Mukai, Y. Matsumoto, Electrophoretic deposition assisted by soluble anode, Mater. Lett. 57 (2003) 2348–2351.
[27] L. Arurault, G. Zamora, V. Vilar, P. Winterton, R. Bes, Electrical behaviour, characteristics and properties of anodic aluminium oxide films coloured by nickel electrodeposition, J. Mater. Sci 45 (2010) 2611–2618.
[28] J.J. Tassel, C.A. Randall, Role of ion depletion in the elecrophoretic deposition of alumina powder from ethanol with increasing quantities of HCl, J. Mater. Sci 41 (2006) 8031–8046.
[29] N. Koura, T. Tsukamoto, S. Hiromasa, T. Hotta, Preparation of various oxide films by an electrophoretic deposition method: a study of the mechanism, Jpn. J. Appl. Phys. 34 (1995) 1643–1647.
[30] L. Stappers, L. Zhang, O. Van der Biest, J. Fransaer, The effect of electrolyte conductivity on electrophoretic deposition, J. Colloid Interface Sci. 328 (2008) 436–446.
[31] G. Anné, B. Neirinck, K. Vanmeensel, O. Van der Biest, J. Vleugels, Origin of the potential drop over the deposit during electrophoretic deposition, J. Am. Ceram. Soc. 89 (2006) 823–828.